

## Time-Resolved X-ray Diffraction Study of Solid Combustion Reactions

JOE WONG, E. M. LARSON, J. B. HOLT, P. A. WAIDE, B. RUPP, R. FRAHM\*

Real-time synchrotron diffraction has been used to monitor the phase transformations of highly exothermic, fast self-propagating solid combustion reactions on a subsecond time scale down to 100 milliseconds and in some instances to 10 milliseconds. Three systems were investigated:  $\text{Ti} + \text{C} \rightarrow \text{TiC}$ ;  $\text{Ti} + \text{C} + x\text{Ni} \rightarrow \text{TiC} + \text{Ni-Ti alloy}$ ; and  $\text{Al} + \text{Ni} \rightarrow \text{AlNi}$ . In all three reactions, the first step was the melting of the metal reactants. Formation of TiC in the first two reactions was completed within 400 milliseconds of the melting of the Ti metal, indicating that the formation of TiC took place during the passage of the combustion wave front. In the Al + Ni reaction, however, passage of the wave front was followed by the appearance and disappearance of at least one intermediate in the afterburn region. The final AlNi was formed some 5 seconds later and exhibited a delayed appearance of the (210) reflection, which tends to support a phase transformation from a disordered AlNi phase at high temperature to an ordered CsCl structure some 20 seconds later. This new experimental approach can be used to study the chemical dynamics of high-temperature solid-state phenomena and to provide the needed database to test various models for solid combustion.

COMBUSTION OF GASEOUS REACTANTS has been actively studied for many years (1). However, the class of combustion reactions in which at least one of the reactants is a solid has received little attention from materials scientists. The products of these "solid flames" are technologically important materials such as ceramics, intermetallics, and composites (2). Solid combustion reactions are universally accompanied by the release of a large amount of heat (3). Once initiated with an external source such as an electrically heated tungsten coil or a laser, these reactions become self-sustained and propagate to completion within seconds. These so-called self-propagating high temperature synthesis (SHS) reactions [or simply solid combustion synthesis (SCS) reactions] are characterized by a fast-moving combustion wave front (1 to 100 mm/s) and a high self-generated temperature (1000 to 4000 K).

Although the basic concepts of this method of material synthesis are relatively easy to apply in principle, there remain many questions concerning the nature of chemical reactions and the dynamics of phase transformations within the combustion wave front (4). This situation is true even with the

most simple  $\text{A} + \text{B} \rightarrow \text{AB}$  combustion reactions. Until recently (5), it has been difficult to investigate these reactions because of the speed and extreme thermal conditions. Wave velocities (6) and temperature profiles (7) could be measured as a function of time and sample position. Examination of the product phase or phases and microstructure was also possible, but the high temperature and fast rates of combustion precluded any in situ investigation of phase transformations and chemical kinetics at the combustion wave front in real time by conventional techniques. To fully exploit the use of solid combustion reactions to process materials, basic mechanisms must be identified. Some of the crucial issues are the role of liquid formation on the combustion process, the effect of intermediate or transient phases on the reaction kinetics, and various extrinsic and intrinsic factors that influence the microstructure of the products.

We have used the high intensity provided by synchrotron radiation and performed a series of time-resolved x-ray diffraction (TR-XRD) experiments (8-12) to follow the chemical reactions and phase transformations in a number of solid combustion systems in situ at high temperatures. A schematic of the apparatus used is shown in Fig. 1. Silicon photodiode arrays manufactured by Princeton Instruments were used as position-sensitive detectors to record the TR diffraction patterns from the specimen ignited

in a specially designed reaction chamber-diffractometer with a vertical  $\theta-2\theta$  geometry ( $\theta$  is the x-ray diffraction angle). Each array is 25 mm long and covers a  $6^\circ$  window in  $2\theta$ -space. The detector is capable of recording a full scan of 1024 pixels in 4 ms. The sample holder and detectors were each positioned with a high-precision Klinger motor-driven stage to enable independent  $\theta$  and  $2\theta$  motions. The sample holder was made of stainless steel and lined with a Grafoil sheet to protect it from corrosion by the hot specimen during combustion. The reaction was initiated (ignited) by the passage of a current through a tungsten (W) coil adjacent to the pressed sample block. A W/W + 26% Re thermocouple placed upstream from a fixed position on the sample illuminated by the synchrotron beam with respect to the propagating combustion wave front was used to trigger the detector at a selected temperature, say,  $1000^\circ\text{C}$ . The diffraction peaks were recorded at a fixed scan rate (for example, 100 ms per scan) for a total number of scans (for example, 1000 scans) with an IBM AT computer. Details of the design and construction of this high-speed time-resolved diffractometer reaction chamber are described elsewhere (13).

The following reactions were selected as model combustion systems in the development of the time-resolved diffraction experimental procedures: reaction 1,  $\text{Ti} + \text{C} \rightarrow \text{TiC}$ ; reaction 2,  $\text{Ti} + \text{C} + x\text{Ni} \rightarrow \text{TiC} + \text{Ni-Ti alloy}$ ; and reaction 3,  $\text{Al} + \text{Ni} \rightarrow \text{AlNi}$ . The choice of these reactions was based on the relatively large volume of experimental data already available on their combustion behavior (14-20). In addition, the products of these reactions are representatives of a ceramic, composite, and intermetallic material, respectively.

The time-resolved diffraction measurements were performed on beam line X-11A at the Brookhaven National Synchrotron Light Source (NSLS) with the x-ray storage ring operating at an electron energy of 2.528 GeV and an injection current of  $\sim 180$  mA. The synchrotron beam, 1 mrad (unfocused) or 2 mrad (focused), passed through a 1-mm entrance slit and was monochromatized with a double Si(111) crystal at 8 keV (wavelength  $\lambda = 1.5497 \text{ \AA}$ ). This energy was chosen to minimize Ni K-fluorescence from the samples in reaction systems 2 and 3, the K-edge of Ni being at 8.333 keV (21). The estimated photon flux for the unfocused beam was  $\sim 10^{10}$  photons per second at the sample plane (22). Before ignition, the chamber was pumped down and back-filled with a He partial pressure of  $\sim 0.5$  bar to avoid oxidation of the metal particles during combustion and to minimize x-ray scattering by air. Diffraction

Lawrence Livermore National Laboratory, University of California, Post Office Box 808, Livermore, CA 94551.

\*On leave from HASYLAB at Deutsches Elektronen-Synchrotron (DESY), Hamburg, West Germany.

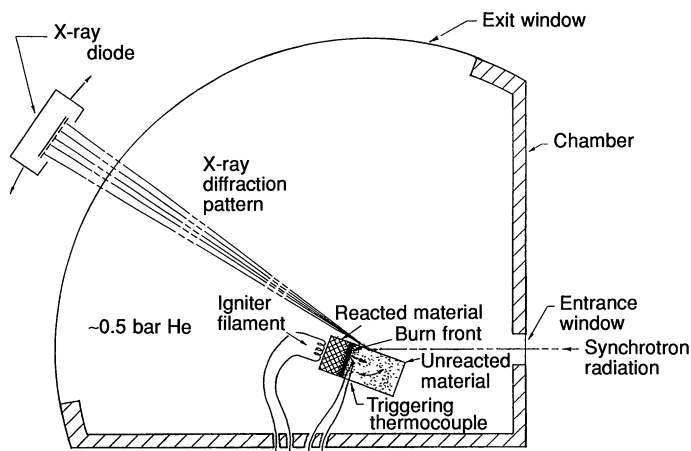


**Fig. 1.** Schematic of the high-speed time-resolved diffractometer reaction chamber used to study solid combustion reactions in situ at high temperature.

specimens in the form of a cube, 19 mm on edge, were pressed from dry-mixed equiatomic mixtures of elemental powders. The average particle size of the Ti, Al, and Ni powders (all from CERAC Inc.) was about 10, 20, and 5  $\mu\text{m}$ , respectively. Submicrometer amorphous carbon procured from CABOT Corporation as a Monarch 900 carbon black was used. The density of the pressed pellets was  $\sim 55$  to 60% theoretical density.

To monitor the formation of TiC in reactions 1 and 2, the  $6^\circ$   $2\theta$  window of one detector was appropriately chosen to cover the strongest diffraction peaks of Ti and the TiC product, that is, the Ti(101) and TiC(200) peaks. The TR diffraction data showed that the time scale for the reaction of the Ti metal and formation of TiC are very similar in both systems within the time

resolution of 200 ms. Therefore, we present only the data for the reaction  $\text{Ti} + \text{C} + 25\% \text{Ni}$  (by weight). For this reaction, 200 scans were made, each taking 200 ms, so that the total scan time for this experiment was 40 s. From the 200 scans, eight representative individual scans were plotted in Fig. 2A to demonstrate the sequence of critical events during combustion. At  $t = 0$  the detector was triggered and recorded the Ti(101) and Ni(111) peaks at room temperature. The intensity of these reactant lines persisted for over 3 s and decreased abruptly at 3.6 s with the simultaneous appearance of the TiC(200) at  $2\theta \sim 41.5^\circ$ . This instant marked the arrival of the wave front at the region of the sample illuminated by the synchrotron beam. From 3.6 s on, the TiC peak grew in intensity until the formation of the TiC phase was completed by 4.0 s.

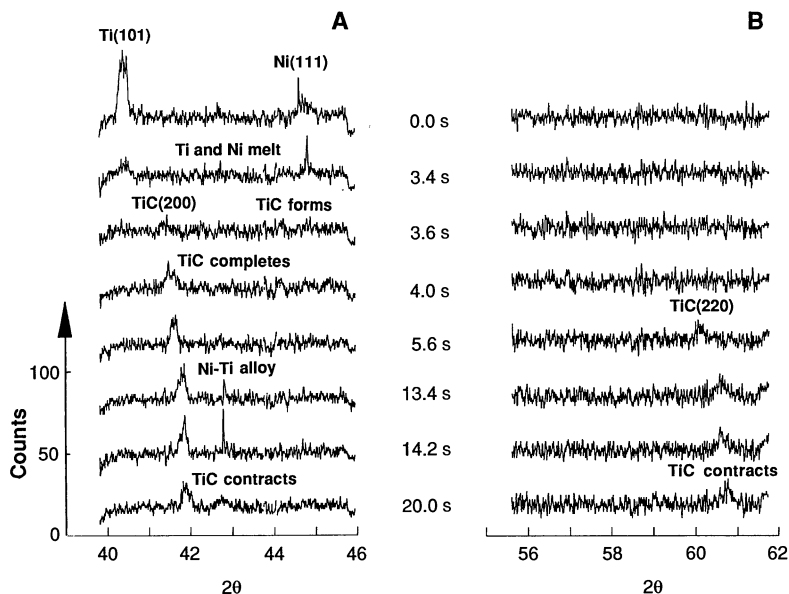


**Fig. 2.** Selected TR diffraction scans of the reaction  $\text{Ti} + \text{C} + 25\% \text{Ni}$  (by weight), showing the sequence of critical events during combustion to form TiC and Ni-Ti alloys. Data were obtained from two separate TR scans: (A) first scan with the detector centered at  $2\theta = 43^\circ$  and (B) second scan with the detector centered at  $2\theta = 59^\circ$ . Scan parameters: 8 keV ( $\lambda = 1.5497 \text{ \AA}$ ), 200 ms per scan, 200 scans;  $t = 0$  corresponds to the triggering of the detector.

Because the wave velocity of this reaction was  $\sim 5 \text{ mm/s}$  (23), formation of the final TiC product took place within the combustion front. The next scan at 5.6 s shows a shift of the TiC(200) peak to higher  $2\theta$  value, indicating lattice contraction caused by the cooling of the reacted specimen.

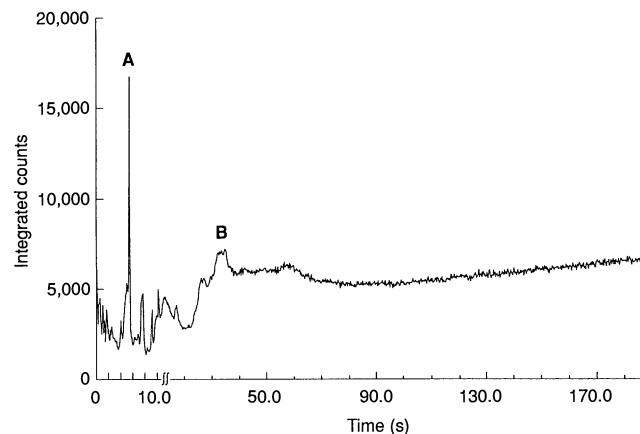
This shift was also observed in the TiC(220) peak recorded in a separate TR experiment on a sister sample with the detector centered at a higher  $2\theta$  angle. The (220) line is a weaker line (60%) in the powder pattern of TiC. It appeared at 5.6 s as shown in Fig. 2B, subsequently shifted to high  $2\theta$ , and persisted till the end of the TR scan at 40 s in the same manner as the TiC(200) peak shown in Fig. 2A. The adiabatic temperature for this reaction was calculated to be  $\sim 2800^\circ\text{C}$  (23), and the W-Re thermocouple recorded a reaction temperature of  $2000^\circ\text{C}$  before failure. The melting points of Ti and Ni are  $1667^\circ$  and  $1455^\circ\text{C}$ , respectively (24). Thus, from this sequence of time-resolved diffraction scans we learn that the first step in the combustion process was the melting of Ti and Ni particles. Subsequently, within the same 200-ms time frame, the molten Ti reacted with the solid C particles to form TiC. It has been suggested (25) that the mechanism of reaction is one of solution-precipitation rather than solid-state diffusion through a growing TiC layer. In this mechanism, the C dissolves in the molten Ti and then precipitates out as TiC grains, which grow in size with time. The total reaction time for the complete formation of TiC was within  $0.4 \pm 0.2 \text{ s}$ . At 13.4 s, a narrow line appeared at  $2\theta \sim 42.7^\circ$  (Fig. 2A), increased in intensity, broadened with time, and persisted as a final reaction product, identifiable as  $\text{Ni}_3\text{Ti}$  or  $\text{NiTi}$ . This finding differs from the result of Dunmead *et al.* (23), who found that, when 25% Ni by weight was added as a diluent in the  $\text{Ti} + \text{C}$  reaction, the final products were TiC and unreacted Ni.

It is known that Ni + Al are stronger x-ray scatterers than Ti + C. Hence, with the Ni + Al intermetallic system we were able to achieve a time resolution of 100 ms using 1 mrad of unfocused beam and of 10 ms using 2 mrad of focused beam. Also, for this system we recorded the TR diffraction patterns simultaneously with two detectors, one centered at  $2\theta = 45^\circ$  to monitor the strongest Ni(111) reactant and the AlNi(110) product peaks, and a second detector centered at  $2\theta = 76^\circ$  to monitor the Ni(220) and Al(311) reactant and the AlNi(210) product peaks. The wave front velocity of this combustion reaction is much higher ( $>20 \text{ mm/s}$ ) than that of the  $\text{Ti} + \text{C}$  reaction. On the basis of a number of survey TR scans, we used two time frames: first at

100 ms for 100 scans to monitor transformations at the arrival of the wave front and then at 200 ms for 900 scans to follow the reaction in the so-called “afterburn” region. The results are shown in Fig. 3.

As before, the detectors were triggered at time  $t = 0$  and the room temperature Ni(111) and Al(200) diffraction peaks were recorded in the low-angle detector as shown in Fig. 3A, and the Ni(220) and Al(311) peaks in the high-angle detector as shown in Fig. 3B. At 0.1 s, all reactant peaks underwent a lowering in intensity, marking the arrival of the combustion wave front in the region of the sample illuminated by the synchrotron beam. The arrival of the wave front within 0.1 s of triggering has been verified by two independent TR scans at 10 and 20 ms. Of particular interest at this instant is the appearance of two diffraction peaks in the low-angle detector, one at the position of room-temperature Ni(111) with reduced intensity and a new one at  $2\theta = 43.8^\circ$ . This new peak may be attributed to a high-temperature Ni peak. Because at  $\theta = 22^\circ$  a 1-mm vertical beam illuminates  $\sim 2.6$  mm of sample, which is much larger than the width of the combustion front, we observed hot Ni as well as Ni in the region near room temperature. Thus, using the known expansion coefficient for Ni (26), one may determine the temperature by measuring the shift in  $d$  spacing (interatomic spacing) of the Ni(111) line. The temperature at that point in the reaction is calculated to be  $\sim 1200^\circ\text{C}$ . At 0.2 s, only the high-

**Fig. 4.** Plot of the integrated intensity from the TR scans shown in Fig. 3A versus time. The region from 0 to 10 s is enlarged to show the high frequency of intensity fluctuations in the first 10 s of the reaction.



temperature Ni peak persisted with increased intensity, indicating that the wave front has completely swept the region illuminated by the x-ray beam. At 0.3 s, the broad Ni diffraction peak was replaced by a number of sharp lines centering at about the same  $2\theta$  region. These sharp lines persisted for over 3 s and may arise from Ni or from an unidentified Ni-Al alloy phase of different grain orientations at high temperature. At 3.6 s, the diffraction intensity from the reacting system fell to a minimum. This was then followed by the appearance of another set of sharp lines centered at  $44.1^\circ$  exhibiting a very high intensity peak at 5.4 s but decreasing sharply in the interval 5.6 to 10 s. At 10.3 s, another cluster of sharp lines centering at  $\sim 44.5^\circ$  appeared, the relative intensities of which vary nonsystematically

with time. These sharp lines and rapid change of their intensities with time could in principle be due to intermediate phases, grain orientation, or grain motion at high temperature, or a combination of all of these effects. This cluster of lines assigned to the (110) reflection of the AlNi product remained for the duration of the diffraction experiment to 190 s, with a shift to high  $2\theta$  value due only to lattice contraction as the reacted specimen cools down. Each multiplex feature observed in the low-angle detector at a given time frame from 5.4 s on arises most likely from a single phase with grains of different orientation within  $\sim 0.25^\circ$ , the geometric resolution of our diffraction setup with a 1-mm slit. Indeed, the number of such sharp peaks within a cluster decreases progressively with reduced slit size from 1 mm to 0.5 mm, and to 0.2 mm. At 31.3 s, the AlNi(210) peak appeared in the high-angle detector (Fig. 3B) and showed also a progressive shift to high  $2\theta$  with time, in a manner similar to that of the AlNi(110) reflection. The appearance of the AlNi(210) peak occurred some 20 s later than that of the AlNi(110) peak. In addition to exhibiting differences in relative intensity [that is, 100% for the (110) peak and 10% for the (210) peak in the powder pattern], this system was characterized by a delay in the appearance of the (210) line, which strongly supports a transformation from a disordered AlNi phase formed at high temperature to an ordered CsCl-structure AlNi phase as it cools.

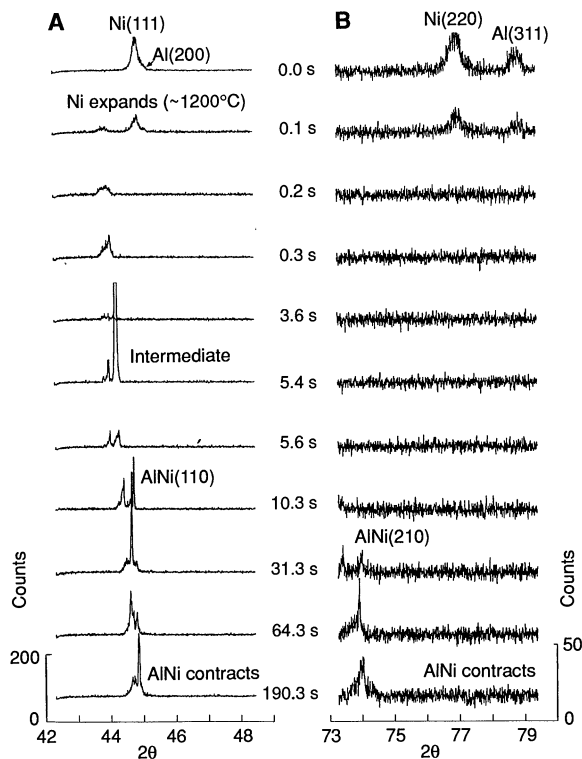


**Fig. 3.** Selected TR diffraction scans of the Al + Ni reaction showing the melting of reactants, the appearance and disappearance of a possible intermediate, and the formation of AlNi as final product. The data were obtained simultaneously with two detectors: (A) one detector centered at  $2\theta = 45^\circ$  and (B) a second detector centered at  $2\theta = 76^\circ$ . Scan parameters: 8 keV ( $\lambda = 1.54975 \text{ \AA}$ ), two time frames successively (i) 10 ms per scan for 100 scans and (ii) 200 ms per scan for 900 scans.

The reported velocity of the combustion front is  $>20$  mm/s for the Al + Ni reaction (21). With a video camera operating at 30 frames per second, we recorded a velocity of 40 mm/s in the above Al + Ni reaction in situ with the TR diffraction experiments. This means that, within 0.5 s of ignition, the wave front has passed through the 19-mm specimen so that the Bragg peaks observed beyond 3.6 s (Fig. 3A) must arise from phases formed after passage of the wave

front, that is, in the afterburn region. The afterburn region is consistent with visual observation of the brightness of the burned sample being sustained for over 30 s and confirms an earlier report by Boldyrev *et al.* (5), who deduced the formation of two intermediates from their TR diffraction experiments in the second time regime.

It is clear from Fig. 3A that most of the observed scattering in the TR diffraction patterns was recorded in the  $2\theta$  region of  $43^\circ$  to  $46^\circ$ . In Fig. 4, the integrated intensity in this  $2\theta$  region is plotted as a function of time. This plot summarizes the TR diffraction events in the combusting Al-Ni system. It is characterized by a very sharp and high-intensity peak, peak A, at 5.4 s with a number of low-intensity peaks on either side. With decreased slit size, the number of these low-intensity peaks decreased as a result of a smaller number of grains correctly oriented to scatter the incident x-ray. This result lends credence to the effect of grain orientation or grain motion, or both, at high temperature on the multiplex features observed with the geometric resolution of our diffraction setup. After 20 s or so, broader peaks such as the one labeled B are observed. Beyond 50 s, the plot becomes almost featureless in accordance to a mere shift of the AlNi(110) product peak to high  $2\theta$  as a result of thermal contraction. Both features at A and B are reproducible in a number of Al + Ni samples repeatedly combusted under identical experimental conditions. Because grain orientation or random motions for individual grains at high temperature would not reproduce the same intensity peaks at the same time in successive scans, the sharp and high-intensity feature observed at 5.4 s is most likely due to an intermediate phase formed before the formation of the final AlNi product.

The technique of TR-XRD with synchrotron radiation is a very powerful and perhaps unique method for following phase transformations and chemical dynamics of solid combustion reactions in situ at high temperature. When temperature profile and wave-front velocity are measured synchronously and correlated with the TR diffraction scans, then all participating phases may be identified as a function of time and temperature. Intrinsic, real-time kinetic data of this sort are needed to allow critical testing of existing theoretical models of solid combustion and to provide the basis for developing new theories. In the case of the Al-Ni systems, there is a great interest in understanding the phase transformation and combustion dynamics as a function of the composition of the starting materials at various stoichiometric as well as off-stoichiometric compositions across the binary sys-

tem (27). Finally, with brighter and higher flux synchrotron sources available currently at wiggler beamlines ( $\sim 10^{12}$  photons per second) or next generation storage rings such as those of the Advanced Light Source (ALS) at Berkeley and the Advanced Photon Source (APS) at Argonne ( $10^{16}$  photons per second), higher spatial resolution should allow a "closer look" at the combustion front in this interesting class of high-temperature solid-state reactions.

#### REFERENCES AND NOTES

1. This is evident from the volume of articles published in *Combustion and Flame* since 1957.
2. Z. A. Munir, *Ceram. Bull.* **27**, 342 (1988).
3. P. Novikov, I. P. Borovinskaya, A. G. Merzhanov, in *Processes in Chemical Engineering and Metallurgy*, A. G. Merzhanov, Ed. (Chernogolovka, 1975), pp. 174-188.
4. Z. A. Munir and U. Anselmi-Tamburini, *Mater. Sci. Rep.* **3**, 277 (1989).
5. V. V. Boldyrev *et al.*, *Dok. Akad. Nauk SSSR* **259**, 1127 (1981).
6. A. G. Merzhanov, *Arch. Procesow Spalania* **5**, 17 (1974).
7. ———, *Arch. Combust.* **1**, 23 (1981).
8. S. M. Gruner, *Science* **238**, 305 (1987).
9. G. Zorn, E. Hellstern, H. Gobel, L. Schultz, *Adv. X-Ray Anal.* **30**, 483 (1987).
10. J. R. Schoonover and S. H. Lin, *J. Solid State Chem.* **76**, 143 (1988).
11. M. Sutton *et al.*, *Phys. Rev. Lett.* **62**, 288 (1988).
12. R. Clark and P. Hernandez, *ibid.*, p. 1768.
13. E. M. Larson, P. A. Waide, J. Wong, *Rev. Sci. Instrum.*, in press.
14. A. S. Rogachev, V. M. Shkuro, I. D. Chauskaya, M. V. Shvetsov, *Fiz. Goreniya Vzryva*, **24** (no. 6), 89 (1987).

15. Yu. S. Naiborodenko and V. I. Itin, *ibid.* **11**, 343 (1975).
16. ———, *ibid.*, p. 734.
17. E. A. Nekrasov, V. K. Smolyakov, Yu. M., Maksimov, *ibid.* **17**, 39 (1981).
18. A. G. Merzhanov *et al.*, *Poroshk. Metall.* **10**, 50 (1981).
19. K. A. Philpot, Z. A. Munir, J. B. Holt, *J. Mater. Sci.* **22**, 159 (1987).
20. J. B. Holt and Z. A. Munir, *ibid.* **21**, 151 (1986).
21. A. Bearden and A. F. Burr, *Rev. Mod. Phys.* **39**, 125 (1976).
22. N. F. Gmur, W. Thomlinson, S. M. White-DePace, *NLSL User's Manual: Guide to the VUV and X-ray Beamlines* (Brookhaven National Laboratory, Upton, NY, ed. 3, 1989).
23. S. D. Dunmead, D. W. Readey, C. E. Semler, J. B. Holt, *J. Am. Ceram. Soc.* **72**, 2318 (1990).
24. R. P. Elliott, *Constitution of Binary Alloys* (McGraw-Hill, New York, 1965), p. 233.
25. V. V. Aleksandrov and M. A. Korchagin, *Fiz. Goreniya Vzryva* **23**, 55 (1987).
26. Y. S. Touloukian, Ed., *Thermophysical Properties of High Temperature Solid Materials* (Macmillan, New York 1967), vol. 1, p. 704.
27. J. Wong, P. A. Waide, J. B. Holt, B. Rupp, E. M. Larson, in preparation.
28. We acknowledge experimental assistance from L. Fareria, J. Scrofani, G. Lambie, S. M. Heald, M. Wilt, and L. Summers. Technical discussions with F. W. Lytle, A. Larson, and L. Tanner are appreciated. This work is supported under the auspices of the U.S. Department of Energy (DOE) by the Lawrence Livermore National Laboratory under contract W-7405-ENG-48. We are also grateful for the support of DOE, Division of Materials Sciences, under contract DE-AS05-80-ER10742, for its role in the development and operation of Beam Line X-11 at the NLSL. The NLSL is supported by DOE, divisions of Materials Sciences and Chemical Sciences, under contract DE-AC02-76CH00016.

13 March 1990; accepted 21 June 1990

## Rapid Determination of the Critical Temperature in Simulated Annealing Inversion

ATANU BASU AND L. NEIL FRAZER\*

Knowledge of the critical temperature,  $T_*$ , the temperature at which a phase change occurs, greatly improves the efficiency of simulated annealing when used for optimization or inversion. A numerical method of accurately determining  $T_*$  in a relatively short computation time has been developed. This method is used to recover the seismic soundspeed profile from wavefield data, a problem in which cycle skipping causes many local minima of the energy function and the averaging of the medium by finite length waves results in many states with similar energies. Computations indicate that it is cost-effective to spend about 80 percent of the computing budget looking for  $T_*$  instead of annealing, and that in the course of finding  $T_*$  many states with energies near the global minimum will also be found. The a posteriori probability distribution of the solution has been constructed from trial solutions generated at  $T_*$ .

**S**IMULATED ANNEALING (SA) WAS INVENTED independently by Kirkpatrick, Gelatt, and Vecchi (1) and by Černý (2). SA makes use of the principle that for a system of particles having random configura-

tions at a fixed temperature  $T$  the probability of finding the system in state  $j$  with energy  $E_j$  is given by the Gibbs distribution

$$g_j = \exp(-E_j/T)/Z \quad (1)$$

in which the partition function  $Z$  is given by a sum over all possible states

$$Z = \sum_i \exp(-E_i/T) \quad (2)$$

Hawaii Institute of Geophysics, University of Hawaii at Manoa, Honolulu, HI 90822.

\*To whom correspondence should be addressed.